Title
THE DECOMPOSITION OF TUNGSTEN-CHROMIUM SOLID SOLUTION

Author
Porter, D.E.

Publication Date
1966-07-01

UCRL-16619 Rev.

University of California
Ernest O. Lawrence Radiation Laboratory

THE DECOMPOSITION OF TUNGSTEN-CHROMIUM SOLID SOLUTION

Berkeley, California

DISCLAIMER

Submitted to Acta Metallurgica

UCRL-16619 Rev
Preprint

UNIVERSITY OF CALIFORNIA

Lawrence Radiation Laboratory
Berkeley, California

AEC Contract W-7405-eng-48

THE DECOMPOSITION OF TUNGSTEN-CHROMIUM SOLID SOLUTION

D. E. Porter

July 1966

THE DECOMPOSITION OF TUNGSTEN-CHROMIUM SOLID SOLUTION

D. E. Porter

Inorganic Materials Research Division, Lawrence Radiation Laboratory,
and Department of Mineral Technology, College of Engineering,
University of California, Berkeley, California

ABSTRACT

The mechanism of solid solution decomposition within the chemical spinodal boundary was investigated for the tungsten-chromium system. Two alloys were solution treated, quenched, and aged at various temperatures inside the chemical spinodal boundary. It was concluded from x-ray and metallographic evidence that tungsten-chromium alloys do not decompose by a spinodal mechanism. The decomposition process was found to be one of nucleation and growth. This observation is in agreement with Cahn's[4] theory of the effect of strain energy on the occurrence of spinodal decomposition.

INTRODUCTION

Tungsten-chromium[1] and molybdenum-chromium[2] are two of the few systems reported in the literature as having a simple miscibility gap in which both decomposition phases are body-centered cubic. Spinodal decomposition is more commonly observed in face-centered cubic systems such as gold-platinum.[3] Cahn[4] has shown that the strain energy of a systems acts to suppress the region where infinitesimal fluctuations (leading to spinodal decomposition) are stable to a supercooled region within the chemical spinodal. To date, little work on solid solution decomposition in body-centered cubic systems has been reported. Experimental verification of the effect of strain energy on the mechanism of decomposition inside the chemical spinodal has not been reported to the knowledge of the author. The lack of information concerning the decomposition mechanisms in body-centered cubic systems, along with the possible technological implications that a high strength, refractory alloy such as tungsten-chromium might have, prompted the present investigation. Investigation of molybdenum-chromium was ruled out for the present time because the top of the miscibility gap is only 900°C and the reaction rates are very slow. Kubaschewski[2] reports reaction times on the order of half a year for alloys of concern in this system.

A portion of the phase diagram for the tungsten-chromium system, with the chemical spinodal boundary drawn in, is shown in Fig. 1. This phase diagram is based on work by Greenaway[1] and was established by x-ray and metallographic methods. The spinodal boundary was calculated from the two-phase boundary using the method of Cook and Hilliard.[5]

EXPERIMENTAL

Tungsten-chromium alloys of two different compositions were investigated (See Fig. 1 for the location of the alloys within the phase diagram). The composition of alloy 1 was 28 atomic percent tungsten, 72 atomic percent chromium, and that of alloy 2 was 39 atomic percent tungsten, 61 atomic percent chromium. These alloys were homogenized at 1750°C for 3 hours, rapidly quenched to room temperature, and reheated to various aging temperatures within the chemical spinodal boundary. The decomposition process was followed by microhardness, x-ray diffraction, and metallographic examinations.

Materials and Sample Preparation

The tungsten and chromium used in this experiment were the purest commercially available in the form of powder (-325 mesh). The approximate percentages of powders for alloys 1 and 2 were weighed and mixed by tumbling for 3 days in a rotary tumbler. These powders were then compacted into 1/4 in. diameter by 1/4 in. long pellets in a tungsten-carbide die at a pressure of 200,000 psi. The pellets were suspended by a tungsten basket in a vacuum furnace, which was then evacuated to 10^{-6} mm Hg and back-filled with purified hydrogen. The hydrogen was purified by passing it over a molecular sieve maintained at liquid nitrogen temperature, then over titanium-zirconium chips maintained at 800°C. The samples were presintered in the purified hydrogen atmosphere at 1000°C for 24 hours in order to remove most of the surface oxygen. Final sintering and solid solution homogenization was carried out on each sample individually. Each sample was suspended in the furnace, evacuated to 10^{-6} mm Hg, and baked out at 700°C for several hours. The furnace was then filled with argon, purified in the way described above for hydrogen,

except using argon boil off to provide the gas. Sintering and homogenization was carried out in one operation by heating the samples for 3 hours at a temperature of 1750°C. After homogenization the samples were rapidly quenched and then aged in one of two ways. Samples aged at temperature below 1100°C were sealed in silica glass under a vacuum of 10^{-6} mm Hg and placed in a tube furnace while samples aged at higher temperatures were heated in a vacuum furnace filled with purified argon.

Apparatus

A high temperature vacuum quenching furnace was designed for maximum quench rates consistent with the use of relatively large specimens. The main features of this system are shown schematically in Fig. 2. The electrodes and carrying tube for the quenching media were fed through the walls of the vaccum chamber in a standard manner. All parts on the vacuum side of the vacuum gate valve (G, Fig. 2) and the parts inside the vacuum chamber were designed to be taken out of the system. These parts could then be washed with acetone and baked out together with the inside of the furnace after each run.

Several heating and quenching schemes were tried. The one described here gave the most consistently good results. A sample was suspended by a tungsten wire basket from the top of quenching nozzle into the center of the heating filament. This filament was constructed of 0.003 in. tantalum foil in the form of an almost closed cylinder 1/2 in. diameter by 1-1/2 in. high. The heating power was supplied by a 0-500 amp, 0-20 v, constant voltage power supply. Distilled water atomized into a high velocity stream of helium was found to give high quenching rates and a minimum of surface contamination (removed by grinding). The control of the quenching cycle proved to be an important issue in determining the

effective quenching rate. To increase consistency in the heating-quench cycle, an electronic control cycle timer was employed. The electronic timer was set so that at the end of the 3 hour sintering-homogenization period, it would trigger power to three circuits -- the first circuit being the solenoid operated water valve, which opens at this time, and the second and third circuits being series arranged time delays. These time delay circuits were simple variable resistance-capacitance triggered solid-state devices. After the water valve was opened there was a delay of 300 milliseconds for the water to reach the atomizing nozzle before the vacuum gate valve was opened. Then there was a delay of 40 milliseconds for the helium-water mixture to reach the specimen before the power was turned off. The latter time delay was needed because without it the temperature would fall a significant amount, due to radiation losses, before the main quench began. A capacitor discharge circuit was needed to supply the initial surge of current to the vacuum solenoid valve. Otherwise it would not open consistently. Quenching rates up to 20,000°C/sec were measured for the specimens used in this investigation.

Techniques

After quenching, the samples were ground and polished. The grain size was small enough that x-ray diffraction investigations could be carried out on the bulk samples in a diffractometer. Specimens were rotated about an axis normal to the axis of the diffractometer in order to obtain more reproducible intensities. Two diffractometer runs were made after each aging treatment. One of the traces was made on the specimen surface as it came out of the furnace or silica glass capsule, and one on a freshly prepared surface. All diffractometer experiments were carried out using Cu K_α radiation. The diffractometer was standardized

for line position and intensity before each experimental run.

An electron beam microprobe was used in conjunction with metallography to identify phases in the early stages of precipitation. Specimens were prepared for metallography by polishing with chrome-oxide and etching electrolytically for 30 sec. in a solution of 2 g NaOH, 20 ml H_2O, and 50 ml glycerin, using a potential of 20 volts.

EXPERIMENTAL RESULTS

Measurements were made on alloys 1 and 2, after aging at various temperatures, using different techniques. Table 1 shows the measurements made with respect to alloy and temperature.

X-ray Diffraction Experiments

Diffraction patterns taken after each quenching and aging treatment failed to show any anomalous diffraction effects. Instead, the normal nucleation and growth sequence was observed during aging. There was no change in intensity or position of the solid solution diffraction lines before the lines due to the new phase appeared. To substantiate the observation that the decomposition process was one of nucleation and growth, an analysis of the diffraction patterns was made to determine the percentage of material transformed as a function of time.

The intensity of the (110) line due to a α phase is:

$$I_\alpha = I_o \cdot (\text{fraction of beam intercepted by the given phase}) \cdot K_{(110)\alpha},$$

$$K_{(110)} = R \cdot \left(\frac{1}{a_o 6}\right) \cdot \left(\frac{1+\cos^2 2\theta}{\sin^2\theta\cos\theta}\right) \cdot \left(\frac{1}{\mu}\right) \cdot \left[(X_{Cr} f_{Cr} + X_W f_W)^2\right]$$

where

R = constant for the (110) line,

a_o = lattice parameter,

θ = Bragg angle,

Table 1. Measurements made on alloys 1 and 2 after aging at various temperatures

Temperature °C	X-ray Diffraction	Microhardness	Metallography
700	Alloy- 1	Alloy- 1	Alloy- 1
900	Alloy- 1		
1000	Alloy- 2		Alloy- 2
1100	Alloy- 1	Alloy- 1	Alloy- 1
1300	Alloy- 1	Alloy- 1	Alloy- 1
1750	Alloys- 1,2	Alloy- 1	Alloy- 1

μ = linear absorption factor,

X_{Cr} = mole fraction of chromium,

X_W = mole fraction of tungsten,

f_{Cr} = atomic scattering factor of chromium,

f_W = atomic scattering factor of tungsten.

The mole fractions of chromium and tungsten for the solid solution and each of the decomposition phases are known, as Greenaway[1] has worked out the variation of lattice parameter with composition. The value of the constant $K_{(110)}$ can be calculated for each phase and temperature of concern. The percentage of the material transformed is then:

$$\% \text{ transformed} = 1 - \frac{\left(I_{\alpha_{ss}} / K_{(110)\alpha_{ss}} \right)}{\left(\frac{I_{\alpha_{ss}}}{K_{(110)\alpha_{ss}}} \right) + \left(\frac{I_{\alpha_1}}{K_{(110)\alpha_1}} \right) + \left(\frac{I_{\alpha_2}}{K_{(110)\alpha_2}} \right)}$$

where α_{ss}, α_1, and α_2 refer to the solid solution and the two decomposition phases respectively.

The (110) line was used for this analysis because it was the most intense line under the conditions used, and the most sensitive to changes in the amount of a given phase present. Typical growth curves obtained from this analysis are shown in Fig. 3. All time-transformation curves show that the decomposition process is one of nucleation and growth. The activation energy for the process (57.5 Kcal/mole) was obtained by plotting the logarithm of the time to half transformation against the reciprocal of absolute temperature, as shown in Fig. 4.

Microhardness

The microhardness data had a relatively large amount of scatter, due

to the extreme hardness, low indenter weight, and porosity of the sample. The mean value of the microhardness (Vickers) is plotted as a function of time along with the coefficient of variation for each point in Fig. 5. This figure shows the high hardness and the moderate hardening potential (approximately 25%) that this alloy possesses.

Metallography

Metallography confirmed the x-ray results, indicating that the decomposition process is one of nucleation and growth. This is shown by micrographs of an aging sequence, for alloy 1, in Fig. 6. The first new phase to appear in the aging sequence, identified by an electron beam microprobe to be the tungsten rich decomposition phase, is seen to grow out from the grain boundaries.

DISCUSSION AND CONCLUSIONS

Alloys that decompose by a spinodal mechanism generally possess three main characteristic features: 1) existence of x-ray side bands in the early stages of decomposition, 2) simple growth characteristics, and 3) random precipitation. None of these features characterizing the spinodal transformation exist in the decomposition of tungsten-chromium alloys. There is no evidence for the existence of side bands. The time-transformation curves show that the decomposition process is not one of simple growth, but rather one of nucleation and growth. The precipitation is not random as in the case of an ideal spinodal decomposition, but rather it is concentrated at the grain boundaries. This x-ray and metallographic evidence indicates that the decomposition process in the tungsten-chromium system is one of nucleation and growth. This conclusion is in agreement with Cahn's[4] theory of the effect of strain energy on spinodal decomposition. Cahn has calculated that the amount of supercooling

necessary for spinodal decomposition of an alloy of critical composition (i.e. an alloy at the top of the miscibility gap) is:

$$T_c - T = \frac{\eta^2 E}{2(1-\nu)kN_v}$$

where T_c = critical temperature (top of miscibility gap),

η = linear expansion per unit composition change,

E = Young's modulus,

ν = Poisson's ratio,

k = Boltzmann's constant,

N_v = number of atoms per unit volume.

The value of η for tungsten-chromium is 0.093, this means a supercooling on the order of 1650°C is needed for spinodal decomposition. This is evidence of the importance of the strain energy term in determining the mechanism of decomposition within the chemical spinodal.

The microstructure of alloy 1 in the later stages of decomposition (Fig. 6) resembles that of lamellar pearlite, such as is found in the iron-carbon system. Earlier work on the tungsten-chromium[1] system also disclosed the lamellar nature of the microstructure. It is reasonable that a lamellar microstructure should develop in the absence of a spinodal decomposition, as a miscibility gap system is, in essence, a simple, unsuppressed eutectoid.

The difference between the bulk and surface time-transformation curves is attributed to the different geometry of the two cases, and not to a change in growth mechanism, as the activation energy is the same for both cases.

ACKNOWLEDGMENTS

The author would like to thank Professor E. R. Parker and Professor V. F. Zackay for their advice and encouragement while undertaking this work. This research was performed under the auspices of the United States Atomic Energy Commission through the Inorganic Materials Research Division of the Lawrence Radiation Laboratory and with the cooperation of the Department of Mineral Technology, University of California, Berkeley.

REFERENCES

1. H. T. Greenaway, J. Inst. Metals 80, 589 (1951-52).
2. O. Kubaschewski and T. G. Chart, J. Inst. Metals 93, 329 (1964-65).
3. L. J. Van der Toorn and T. J. Tiedema, Acta Met., 8, 711 (1960); and L. J. Van der Toorn and T. J. Tiedema, Acta Met., 8, 715 (1960).
4. J. W. Cahn, Acta Met., 9, 795 (1961).
5. H. E. Cook and J. E. Hilliard, Trans. AIME 233, 142 (1965).

FIGURE CAPTIONS

Fig. 1 Phase diagram for the tungsten-chromium system with the chemical spinodal boundary drawn in.

Fig. 2 Schematic view of heating-quenching apparatus.

Legend: A high current, water cooled power leads

B water-cooled heating filament clamp

C electrical insulation

D specimen

E refractory metal heating filament

F carrying tubes for quenching media

G solenoid-operated vacuum gate valve

H atomizing nozzle

I needle-valve for control of water flow

J solenoid valve

K container holding distilled water under gas pressure

L large surge tank

Fig. 3 Time-transformation curve for 900°C.

Fig. 4 Logarithm of the time to half transformation plotted against the reciprocal of the absolute temperature.

Fig. 5 Vickers hardness as a function of time at 700, 1100, and 1300°C. The coefficient of variation is given with each experimental point.

Fig. 6 Micrographs of alloy 1 as solution-treated, quenched, and aged for:

a. 10 min. at 1100°C

b. 817 min. at 1100°C

c. 10,332 min at 1100°C

d. 10,332 min. at 1100°C

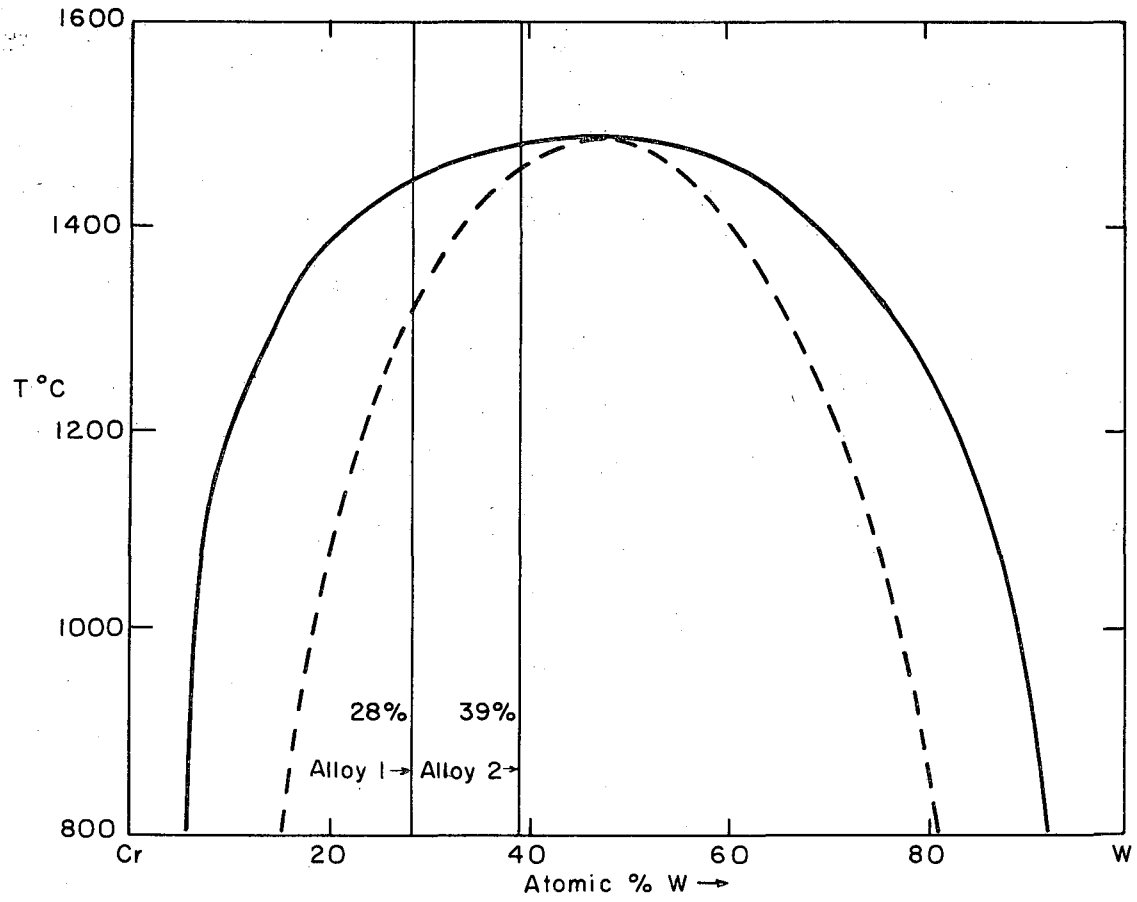

MUB-11341

Fig. 1

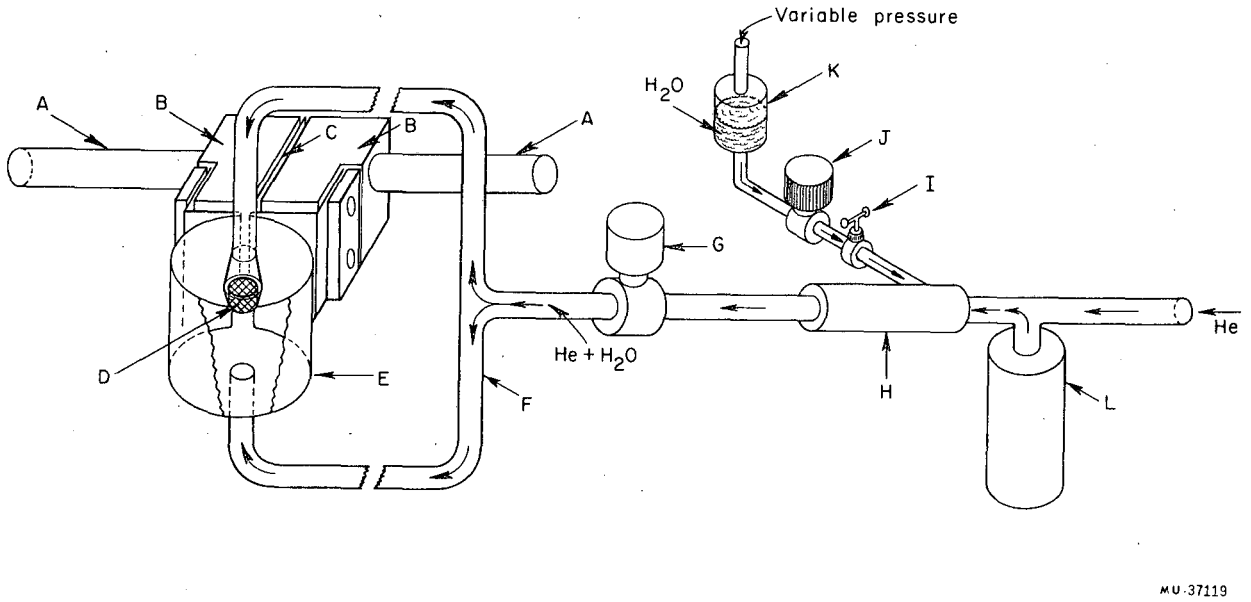

Fig. 2

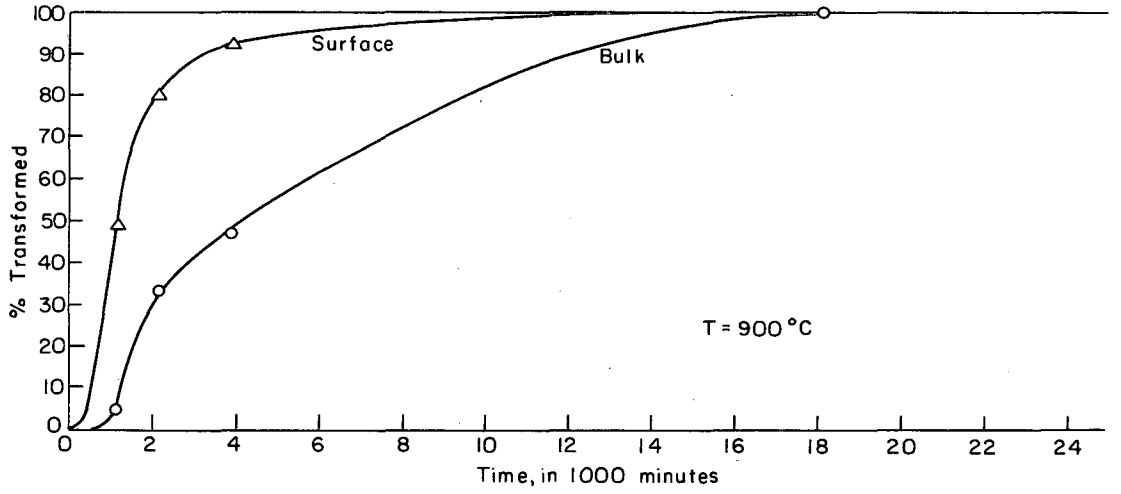

MUB-11342

Fig. 3

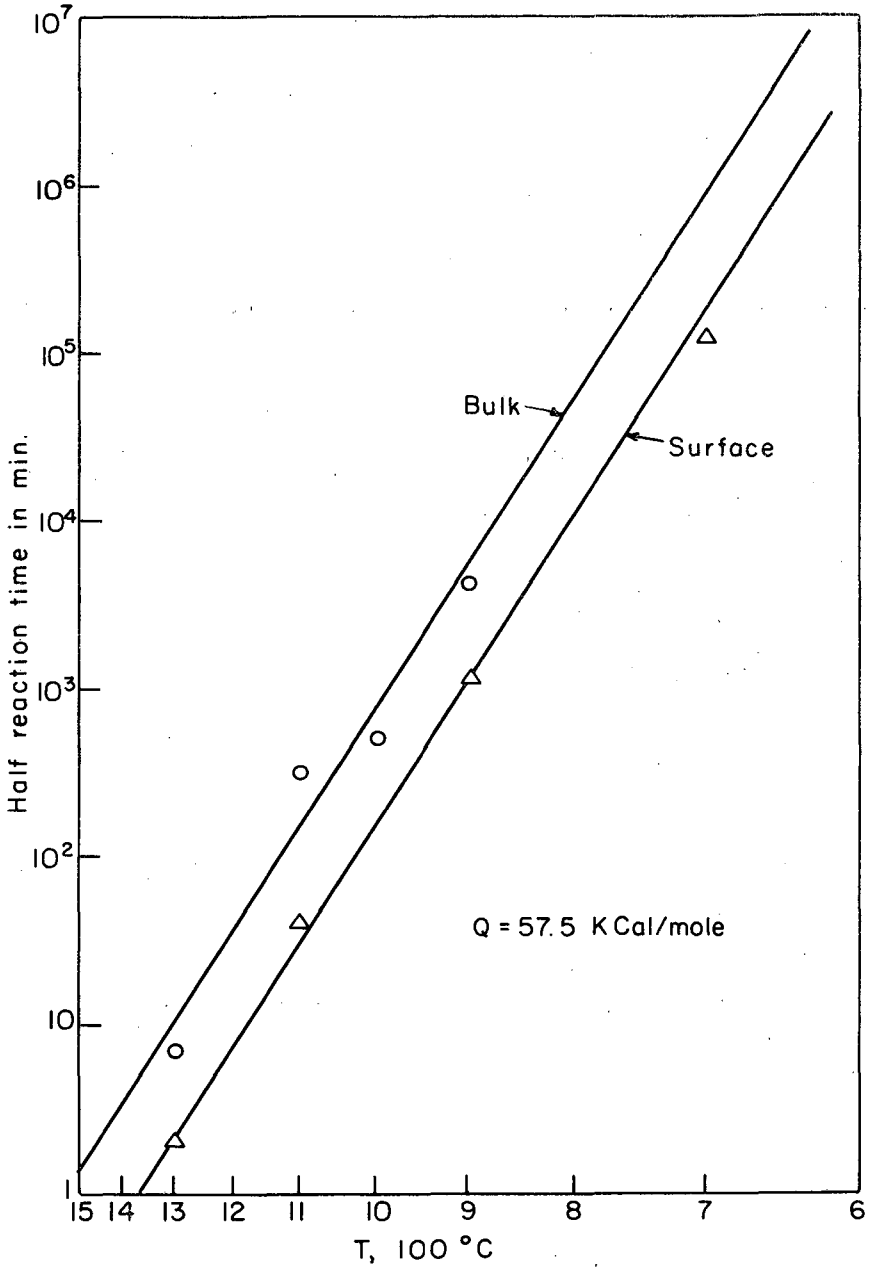

MUB-11343

Fig. 4

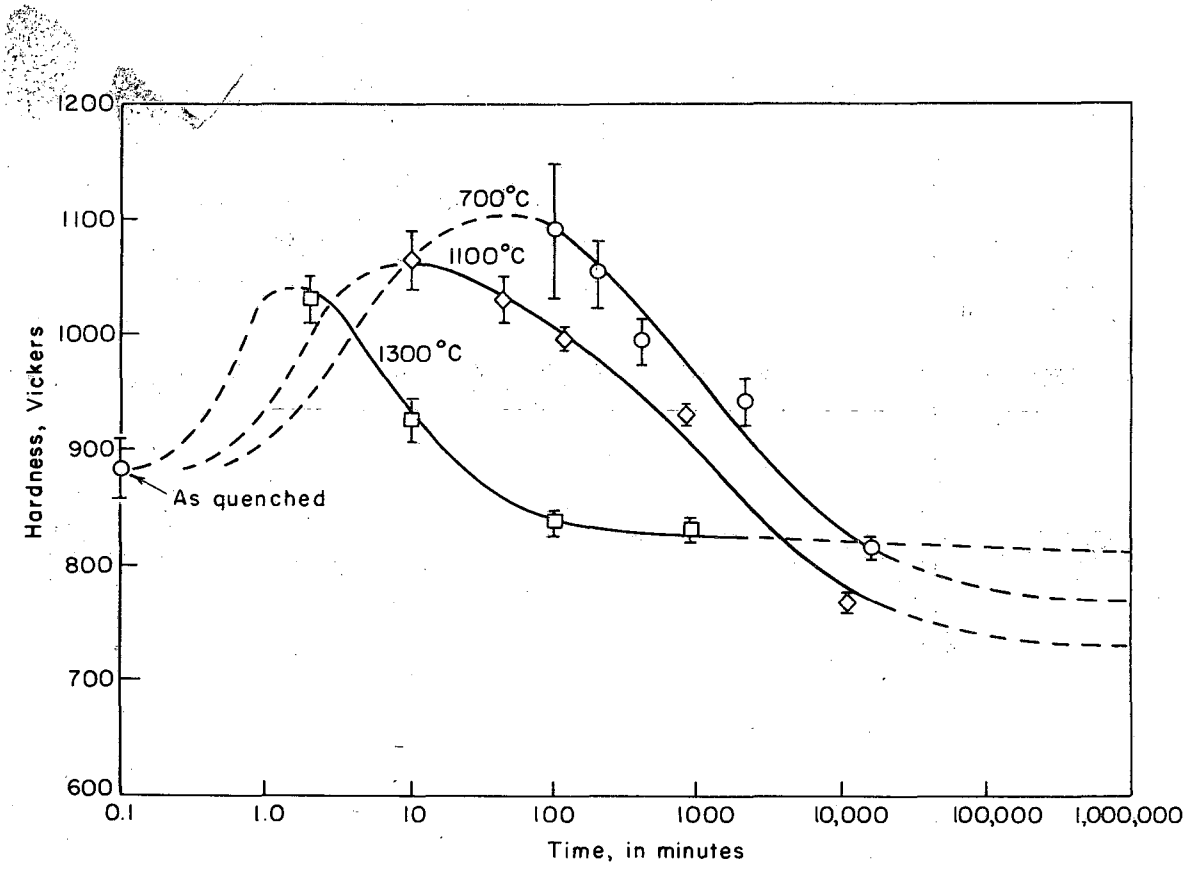
1200
1100
1000
900
800
700
600
Hardness, Vickers
700°C
1100°C
1300°C
As quenched
0.1
1.0
10
100
1000
10,000
100,000
1,000,000
Time, in minutes
MUB-11344

Fig. 5

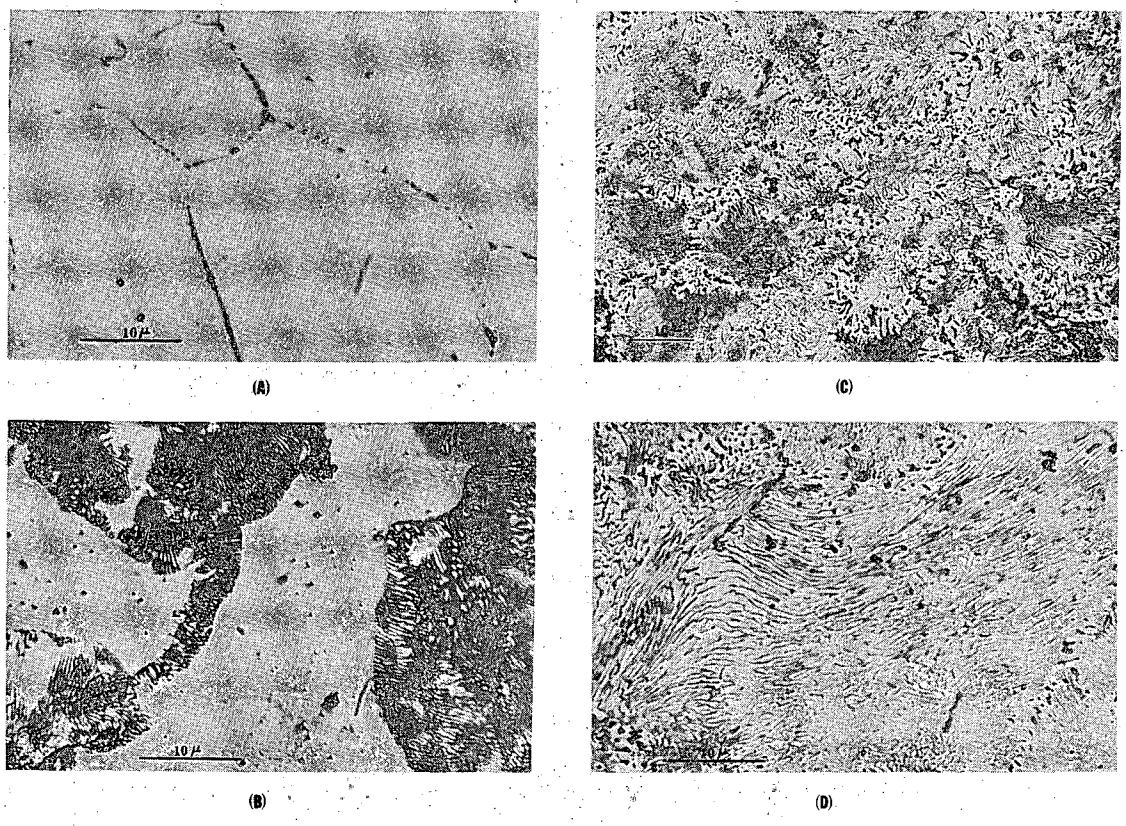

ZN-5697

Fig. 6